Molecular Therapy
Methods & Clinical Development
Original Article

Virally mediated enhancement of efferent inhibition reduces acoustic trauma in wild-type murine cochleas

Eleftheria Slika,[1] Paul A. Fuchs,[1] and Megan Beers Wood[1]

[1]Department of Otolaryngology-Head and Neck Surgery, Johns Hopkins University School of Medicine, Baltimore, MD 21205, USA

Noise-induced hearing loss (NIHL) poses an emerging global health problem with only ear protection or sound avoidance as preventive strategies. The cochlea receives some protection from medial olivocochlear efferent neurons, providing a potential target for therapeutic enhancement. Cholinergic efferents release acetylcholine (ACh) to hyperpolarize and shunt the outer hair cells (OHCs), reducing sound-evoked activation. The $(\alpha9)_2(\alpha10)_3$ nicotinic ACh receptor (nAChR) on the OHCs mediates this effect. Transgenic knockin mice with a gain-of-function nAChR (α9L9′T) suffer less NIHL. α9 knockout mice are more vulnerable to NIHL but can be rescued by viral transduction of the α9L9′T subunit. In this study, an HA-tagged gain-of-function α9 isoform was expressed in wild-type mice to reduce NIHL. Synaptic integration of the virally expressed nAChR subunit was confirmed by HA immunopuncta localized to the postsynaptic membrane of OHCs. After noise exposure, AAV2.7m8-CAG-α9L9′T-HA (α9L9′T-HA)-injected mice had less hearing loss (auditory brainstem response [ABR] thresholds and threshold shifts) than did control mice. ABRs of α9L9′T-HA-injected mice also had larger wave-1 amplitudes and better recovery of wave-1 amplitudes post noise exposure. Thus, virally expressed α9L9′T combines effectively with native α9 and α10 subunits to mitigate NIHL in wild-type cochleas.

INTRODUCTION

With the ever-accelerating use of personalized sound devices and urban exposure to high sound-pressure levels (SPLs), noise-induced hearing loss (NIHL) is arising as a major health problem worldwide. In their 2021 report, the World Health Assembly predicts that by 2050 almost 2.5 billion people will suffer from hearing loss.[1,2] In 2019, 1.57 billion people suffered to some degree from hearing loss, equivalent to 43.45 million years lived with disability, making hearing loss the third-largest cause of global disease burden. This corresponds to more than $981 billion in total costs, with most of this burdening populations from lower socioeconomic groups and older age.[3–5] Noise exposure, either occupational or social, accumulates over one's lifespan, promoting sensory hair cell damage and loss of auditory function.[6] It is a major cause of sensorineural hearing loss and contributes to the development of age-related hearing loss.[7] According to Centers for Disease Control and Prevention data from 2011 to 2012, audiometric evidence of noise-induced hearing loss appears in up to 24% of adults 20–69 years old.[8] Over 100 million people are exposed to damaging noise levels in the United States.[9] Aside from protective devices and avoidance of loud sounds, there are no Food and Drug Administration-approved therapies to prevent noise-induced damage to the ear.[7] Here, we will describe how inner-ear gene therapy can enhance a native reflex of the cochlear apparatus to mitigate noise-induced hearing loss *in vivo*. This approach will be of particular benefit for those at risk of early-onset age-related hearing loss. This also is an alternative strategy for gene therapy, not to replace a defective gene but to enhance the function of a native neuronal circuit by addition of a gain-of-function isoform.

The medial olivocochlear reflex provides efferent innervation from the superior medial olivary complex in the brainstem to the sensory epithelium of the cochlea, the organ of Corti.[10,11] Prior to hearing onset in mammals, cholinergic medial olivocochlear fibers synapse with and inhibit inner hair cells (IHCs), contributing to the differentiation and functional maturation of the IHC afferent synapses.[12–14] As the IHCs and outer hair cells (OHCs) differentiate, medial olivocochlear fibers migrate from the inner to the outer hair cell region, where they form inhibitory synapses on OHCs. By hearing onset, the medial efferent fibers synapse only with the OHCs. The medial olivocochlear locus in the brainstem receives frequency-tuned input from bilateral cochlear nuclei to activate efferent fibers in response to elevated sound levels. The pharmacology of the medial olivocochlear synapse involves the $(\alpha9)_2(\alpha10)_3$ nicotinic receptor, which is activated by the binding of two acetylcholine molecules on the α9 subunits.[15–17] Upon medial efferent activation, acetylcholine (ACh) release binds the nicotinic ACh receptor (nAChR) and induces an inward Ca^{2+} current, which, in turn, activates SK and BK Ca^{2+}-dependent K^+ channels.[18,19] This increase in membrane permeability to K^+ hyperpolarizes the OHCs and shunts their electromotility, thus preventing noise-induced overactivation.

Received 10 October 2024; accepted 18 March 2025;
https://doi.org/10.1016/j.omtm.2025.101455.

Correspondence: Eleftheria Slika, Department of Otolaryngology-Head and Neck Surgery, Johns Hopkins University School of Medicine, Baltimore, MD 21205, USA.
E-mail: eslika1@jhmi.edu

The medial olivocochlear system acts with frequency and sound-level specificity to fine tune OHC electromotility and prevent over-excitation. Several studies have shown that it can act as a protective mechanism against noise-induced hair cell damage.[20–31] Substituting a threonine for a leucine at position 9′ (L9′T) of the second transmembrane domain of the α9 subunit produces an α9L9′T isoform with increased sensitivity to ACh and prolonged mean open times of the channel.[32] This results in enhanced magnitude and duration of the medial olivocochlear (MOC) effect.[33] Studies on transgenic knockin mice for the gain-of-function α9L9′T isoform showed that they were better protected from noise-induced threshold shifts than the wild-type (control) group for the same noise exposure. In contrast, transgenic α9 knockouts, lacking MOC feedback, were more vulnerable to noise-induced threshold shifts than were wild type.[20] Viral transduction of the α9L9′T isoform into α9 knockout mice spared them from the temporary threshold shifts that their uninjected α9 knockout littermates suffered after noise exposure.[31] Fluorophore-conjugated conopeptides showed expression of the α9L9′T nAChR on the synaptic membrane of α9 knockout OHCs.

Adeno-associated virus 2.7m8 (AAV2.7m8) efficiently transduces all types of neuroepithelial cells in the cochlea, including both IHCs and OHCs.[34] For visualization of the α9 subunit on fixed tissue through immunolabeling, a hemagglutinin (HA) tag was attached to the C terminus of the α9 sequence. This HA-tag position was shown previously not to reduce receptor function in α9-HA heterozygous mice.[35]

In this study, the α9L9′T-HA sequence (expressed under a CAG promoter in AAV2.7m8, Figure 1A) was introduced into wild-type cochleas through posterior semicircular canal injections. C57BL/J6 mice (ten females and nine males) were injected with AAV2.7m8-CAG-α9L9′T-HA (α9L9′T-HA) at postnatal days 1–5 and noise exposed at 5 weeks of age. The aim was to express the α9L9′T-HA subunit on the OHC postsynaptic membrane for interaction with native α9 and α10 to form functional heteromeric nAChRs, thus enhancing MOC feedback and increasing protection against noise-induced trauma.

RESULTS

α9L9′T-HA is expressed on the postsynaptic membrane of OHCs

Immunofluorescent labeling of the HA tag of the virally introduced gain-of-function α9 subunit showed widespread expression along the cochlear spiral (magenta, Figure 1C). This was combined with presynaptic labeling of the efferent fibers by an SV2 antibody (green, Figure 1C), along with DAPI, which labels cell nuclei (blue, Figure 1C). HA puncta juxtaposed to SV2-positive efferent terminals were found on the basal pole of OHCs, near the nucleus. This corresponds to the known efferent contacts on OHCs[10,11,15–18] indicating that the viral protein is localized as expected for the α9α10 nAChR. Quantification of the fraction of OHCs with HA synaptic puncta in confocal images from each cochlear region (Figure 1D) showed a declining gradient from apex to base in the injected (left) cochleas. Starting at the apical turn, the percentage of HA-positive OHCs declined from 78% to just 7% in the basal-most hook.

Synaptic HA puncta are absent from adult IHCs,[12] but there was substantial diffuse cytoplasmic HA immunolabel. The high AAV2.7m8 transduction efficiency and strong CAG promoter, as shown previously,[34] drove expression of green fluorescent protein (GFP) in the cytoplasm of IHCs and supporting cells, confirming successful injection, viral transduction, and patterns of expression for these preparations. As with OHC expression, the IHC cytoplasmic HA label declined from apex to base, from 87% in the apex to 27% in the basal-most hook region (Figure 1E).

Limited HA label also was observed in the contralateral (uninjected) cochlea (Figure 1F). In contrast to the injected side, HA labeling was confined mainly to the basal regions of the uninjected ear. Cytoplasmic HA label declined steeply from 36% of IHCs at the base to just 7% at the middle turn and none at the apex. OHC postsynaptic HA puncta were seen in only one OHC in the basal segment of each of two contralateral cochleas.

Baseline ABR thresholds and wave-1 amplitudes of the α9L9′T-HA vs. the uninjected control group were slightly elevated

Viral injections were administered into the left posterior semicircular canal of C57Bl/J6 mouse pups at postnatal days 2–5 (P1–P5). The experimental group included 19 α9L9′T-HA-injected C57Bl/J6 wild-type mice. The control groups included 14 uninjected and 8 AAV2.7m8-CAG-eGFP (enhanced GFP)-injected littermates.

Baseline ABRs (before noise exposure) were recorded from the left (injected) side of 5-week-old animals for clicks and pure tones at 8, 12, 16, 24, 32, 40, and 46 kHz (Figure 2). Pairwise comparisons of click and pure-tone thresholds found no significant differences between α9L9′T-HA-injected and control groups (Kruskal-Wallis test for clicks, non-normal distribution; multiplicity adjusted p values with Tukey's multiple comparisons test after two-way ANOVA for pure-tone frequencies, Figure 2A). However, two-way ANOVA did show significance between groups ($F(2, 266) = 5.165$, $^{**}p < 0.01$) across pure tones. The mean difference in threshold between α9L9′T-HA and uninjected groups was 6 dB (95% confidence interval [CI] 2–10 dB; $^{**}p < 0.01$). However, mean thresholds did not differ significantly between the α9L9′T-HA and the GFP-injected groups (1 dB, 95% CI −4 to 7 dB) or between the uninjected and GFP-injected groups (−4 dB, 95% CI −10 to 1 dB) (multiplicity adjusted p values with Tukey's multiple comparisons test).

Baseline click wave-1 amplitudes at 80 dB were not significantly different among the groups (ordinary one-way ANOVA, Figure 2B). However, two-way ANOVA for wave-1 amplitude of pure tones up to 24 kHz did show significance among groups ($F(2, 152) = 7.041$, $^{**}p < 0.01$). As for thresholds, only α9L9′T-HA vs. uninjected overall mean difference (−0.57 μV) is significant, whereas the α9L9′T-HA vs. GFP difference (−0.169 μV) and the uninjected vs. GFP (−0.4 μV) are not (multiplicity adjusted p values with Tukey's multiple comparisons test). Pairwise comparisons for pure-tone wave-1 amplitudes showed significance between the α9L9′T-HA and the

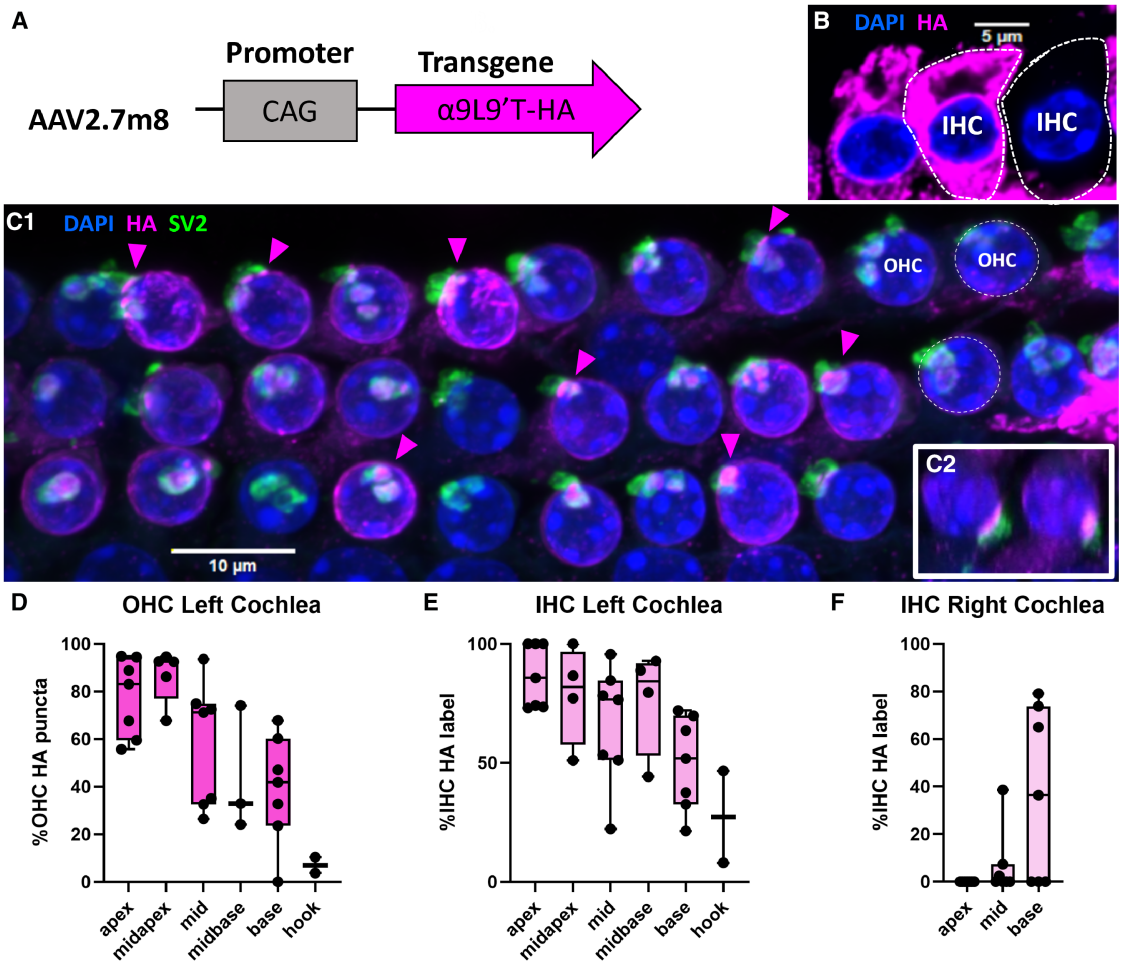

Figure 1. Viral transduction of cochlear α9L9′T-HA expression

(A) Schematic of AAV2.7m8 bearing the α9L9′T-HA sequence under a strong universal promoter. (B) Representative image of the IHC row of the left basal turn of a 7-week-old C57Bl/J6 wild-type male mouse injected at P3 with 600 nL of AAV2.7m8-CAG-α9L9′T-HA viral solution. IHCs with HA cytoplasmic label in magenta and nuclei stained in blue with DAPI. IHC margins are outlined with white dashed lines. (C1) Maximal intensity projection image of the three OHC rows (1 nucleus in each row indicated by white dashed lines) of the left middle turn of a 7.5-week-old C57Bl/J6 wild-type female mouse injected at P3 with 900 nL of AAV2.7m8-CAG-α9L9′T-HA viral solution. Immunofluorescent secondary antibodies label dense HA puncta (magenta, some indicated by arrowheads) on the OHC postsynaptic membrane juxtaposed to SV2-positive (green) presynaptic terminals, showing synaptic localization of the virally encoded α9 subunit. OHC and supporting cell nuclei are labeled with DAPI (blue). (C2) Resliced image on the z axis of two OHCs of the same region with (C1), where the HA label appears on the postsynaptic density at the basal pole of the OHC, juxtaposed to the SV2-labeled presynaptic terminal. (D–F) HA expression gradient along the cochlear spiral of seven mice (five males and two females). (D) Percent (mean ± maximum, minimum, and individual values) of OHCs with postsynaptic HA expression in seven left (injected) cochleas: apex 7 segments, 847 OHCs; mid apex 5 segments, 717 OHCs; mid 7 segments, 903 OHCs; mid base 3 segments, 459 OHCs; base 7 segments, 794 OHCs; hook 2 segments, 197 OHCs. (E) Left (injected) cochlea ($N = 7$) percentage (mean ± maximum, minimum, and individual values) of IHC with HA cytoplasmic label: apex 7 segments, 199 IHCs; mid apex 4 segments, 157 IHCs; mid 7 segments, 257 IHCs; mid base 4 segments, 179 IHCs; base 7 segments, 271 IHCs; hook 2 segments, 70 IHCs. (F) Percentage of IHC (mean ± maximum, minimum, and individual values) with HA cytoplasmic label in seven right (contralateral to injected) cochleas, 675 IHCs.

uninjected group at 8 kHz and between the uninjected and GFP-injected mice at 16 kHz.

These baseline data suggest a slight threshold elevation due to expression of α9L9′T-HA, as reported previously,[33] but this was evident only from 8 to 16 kHz. Thresholds for the highest frequencies tested were slightly, but not significantly, elevated for both α9L9′T-HA- and GFP-injected mice. Likewise, baseline wave-1 amplitudes were minimally affected by viral injection *per se* (GFP-injected vs. uninjected). In contrast, viral transduction with α9L9′T-HA markedly altered the response to acoustic trauma.

Post acoustic trauma, the α9L9′T-HA group had lower thresholds and threshold shifts compared to controls

All animals were exposed at 5 weeks of age to an 8- to 16-kHz octave-band signal at 100 dB for 1 h (gray band in Figure 3). Post-exposure

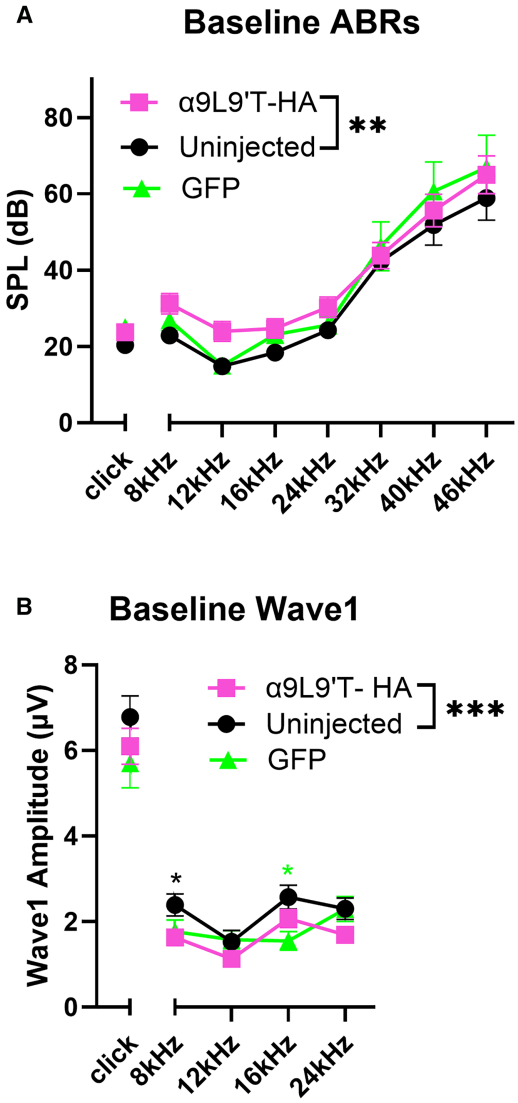

Figure 2. Baseline ABR thresholds and click wave-1 amplitude

ABR recordings pre-exposure for all groups (mean ± SEM). C57Bl/J6 wild-type mice, 5 weeks old. α9L9′T-HA injected group, *N* = 19 (magenta) vs. the uninjected group, *N* = 14 (black) vs. GFP-injected group, *N* = 8 (green). Black asterisks for uninjected vs. α9L9′T-HA, magenta asterisks for GFP vs. α9L9′T-HA, green asterisks for GFP vs. uninjected. (A) ABR thresholds at baseline. Kruskal-Wallis test for click thresholds and two-way ANOVA for pure tones with multiplicity adjusted *p* values after Tukey's multiple comparisons test. (B) 80-dB wave-1 amplitudes at baseline. Ordinary one-way ANOVA for clicks and two-way ANOVA for pure tones with multiplicity adjusted *p* values after Tukey's multiple comparisons test. $^{*}p < 0.05$, $^{**}p < 0.01$, $^{***}p < 0.001$, $^{****}p < 0.0001$; ns not significant.

ABR threshold values and shifts from baseline were plotted for clicks and individual frequencies (8, 12, 16, 24, 32, 40, and 46 kHz) at 1, 7, and 14 days post trauma (Figure 3). For all time points, two-way ANOVA showed significantly lower absolute thresholds and threshold shifts for the α9L9′T-HA group compared to GFP-injected and uninjected controls (Figure 3). GFP-injected and uninjected ears showed similar patterns of acoustic damage. In contrast to the two control groups, the α9L9′T-HA-injected group not only had 1-day post-trauma thresholds significantly lower than the controls, but there was also better recovery at 7 and 14 days after trauma. This is shown by the threshold shift graphs (Figures 3D–3F), which present a pattern like that for absolute thresholds. α9L9′T-HA-injected shifts were the smallest, and GFP-injected shifts were not different from those of the uninjected mice.

Additional features were revealed by within-group comparisons (Figure 4). The α9L9′T-HA-injected group experienced a smaller (mean 15 dB above baseline) threshold shift compared to controls (Figure 4). Also, the α9L9′T-HA injected group recovered progressively from 1 to 14 days post trauma. Indeed, at 14 days post exposure, the click, 8-, 12-, 16-, 40-, and 46-kHz absolute thresholds did not differ significantly from the pre-exposure baseline (Figure 4A). The 12- to 24-kHz area showed the maximal difference between the α9L9′T-HA and the control groups initially, with better recovery as time progressed. Threshold shifts at 1, 7, and 14 days were progressively smaller and significantly different from each other for pure tones and clicks (Figure 4D).

Repeated-measures two-way ANOVA for pure-tone threshold shifts (Figures 4D–4F) with Tukey's multiple comparisons for overall group means yielded significant *p* values between 1 and 7 days for both the uninjected and the GFP-injected animals, indicating partial recovery at 7 days. However, there was no further improvement at 14 days, suggesting a degree of permanent threshold shift (PTS). At 14 days, the mean threshold elevation was 36 dB for the uninjected group and 33 dB for the GFP-injected group (vs. 15 dB for the α9L9′T-HA group). Click threshold shift comparisons among 1-, 7-, and 14-day values were not significant for both control groups (Friedman's test and Dunnett's test for multiple comparisons), emphasizing that there was minimal threshold recovery after the initial 1-day damage.

Post acoustic trauma, click and pure-tone wave-1 amplitudes at 80 dB are largest for the α9L9′T-HA group

Wave-1 amplitude for clicks and pure tones was measured for all mice prior to and then 1, 7, and 14 days after acoustic trauma (Figure 5). For all groups, click wave-1 amplitude at 80 dB SPL was halved 1 day post exposure. For the control groups, click amplitudes did not recover and remained significantly smaller, around half of baseline values (Figures 5D–5F, repeated-measures one-way ANOVA with Dunnett's multiple comparisons between group means, multiplicity adjusted *p* values). However, α9L9′T-HA click amplitudes at 80 dB were significantly larger than controls at 14 days (Figures 5A–5C and 6), indicating that the α9L9′T-HA injections resulted in click amplitude recovery, which the control groups lacked (ordinary one-way ANOVA with Tukey's multiple comparisons test). For the uninjected mice, baseline mean at 14 days was 3.21 μV, vs. 6.78 μV before trauma. For the GFP group, amplitude fell from 5.7 μV to 2.93 μV at 14 days. However, the α9L9′T-HA group showed excellent recovery, with a 14-day click amplitude mean of 5.13 μV, not significantly different from baseline (6.1 μV) (Figure 5D).

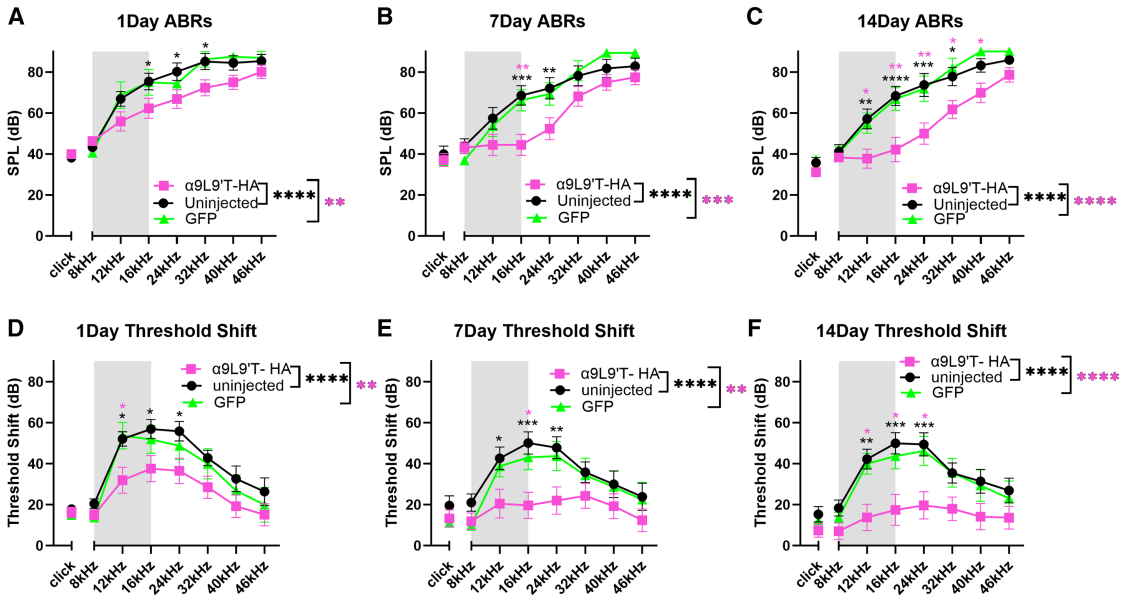

Figure 3. Post-exposure ABR absolute thresholds and threshold shifts from baseline

(A–C) ABR absolute thresholds and (D–F) threshold shifts from baseline. All animals were exposed to an octave-band (8–16 kHz) stimulus at 100 dB for 1 h, represented by the gray area on the frequency band. α9L9′T-HA-injected group $N = 19$ (magenta), uninjected group $N = 14$ (black), GFP-injected group $N = 8$ (green). Black asterisks for uninjected vs. α9L9′T-HA, magenta asterisks for GFP vs. α9L9′T-HA, green asterisks for GFP vs. uninjected. Values are mean ± SEM. $^{*}p < 0.05$, $^{**}p < 0.01$, $^{***}p < 0.001$, $^{****}p < 0.0001$; ns, not significant. Ordinary one-way ANOVA (if normality present) or Kruskal-Wallis test (if non-normal data) for clicks, no significance at any time point. Two-way ANOVA for pure tones with multiplicity adjusted p values with Tukey's multiple comparisons test for overall group means and individual frequency comparisons.

In a similar pattern, pure-tone 80-dB wave-1 amplitude analysis of group means showed that α9L9′T-HA amplitudes were significantly larger than those of the uninjected mice at 7 and 14 days (Figures 5A–5C). Especially at 14 days, pure-tone wave-1 amplitudes for the α9L9′T-HA group were larger than for both uninjected and GFP-injected groups (two-way ANOVA with Tukey's multiple comparisons test). For individual frequency comparisons (multiplicity adjusted p values with Tukey's test), the 16- and 24-kHz frequencies showed larger amplitudes and enhanced recovery for the α9L9′T-HA group than for controls (Figures 5A–5C). Within-group analysis (Figures 5D–5F) showed that 1 day after acoustic trauma, wave-1 amplitude at 80 dB was reduced significantly in all cohorts. On subsequent days the α9L9′T-HA-injected mice showed improvement. Wave-1 amplitude at 7 days and 14 days post exposure increased gradually from the small 1-day values for frequencies above 12 kHz, returning nearly to baseline at 14 days. In contrast, wave-1 amplitude of both GFP-injected and uninjected mice had no significant recovery 14 days post trauma (Figures 5D–5F and 6).

Of note, the 8- to 12-kHz frequency band was not affected by the octave-band exposure, thus wave-1 amplitudes at 80 dB of these tones remained the same at all time points for all groups. Similarly to ABR thresholds, maximal damage was located at the 16- to 24-kHz area, with only the α9L9′T-HA group showing amplitude recovery at 14 days.

IHC synapse counts show no significant difference in the α9L9′T-HA-injected cochleas vs. controls post exposure

After concluding ABR recordings, the animals were sacrificed at 15–17 days post noise exposure, and the synaptic puncta of IHC type I afferents were analyzed. For visualization of IHC afferent synapses, immunofluorescent labeling of presynaptic ribbons (anti-CtBP2) and postsynaptic densities (anti-PSD95) was performed. Confocal microscopy images from the apical, middle, and basal turns of each cochlea were acquired, with 15–30 IHC nuclei counted in each image. The total number of juxtaposed CtBP2/PSD95 puncta in each image was counted and divided by the number of IHC nuclei. Synapses/IHCs are plotted for the apical, middle, and basal cochlear regions of the α9L9′T-HA-injected left cochleas ($N = 3$, magenta) and their contralateral right cochleas ($N = 3$, pink) and compared with the left cochleas of uninjected mice ($N = 6$, gray) (Figure 7). Two-way ANOVA showed no significant interaction between the three groups ($F(4, 27) = 2.1$, $p > 0.05$). This observation could be attributed to the small number of mice studied. If validated in a larger group of animals, it could mean that this acoustic protocol does not necessarily cause morphological IHC synapse loss in these animals at this time point. Rather, this suggests that the observed reduction in wave-1 amplitude is due to an as yet undefined decrement in synaptic function. This could be of pre- or postsynaptic origin, and other structures in the organ of Corti could be damaged, affecting the activation of the afferent cochlear fibers.

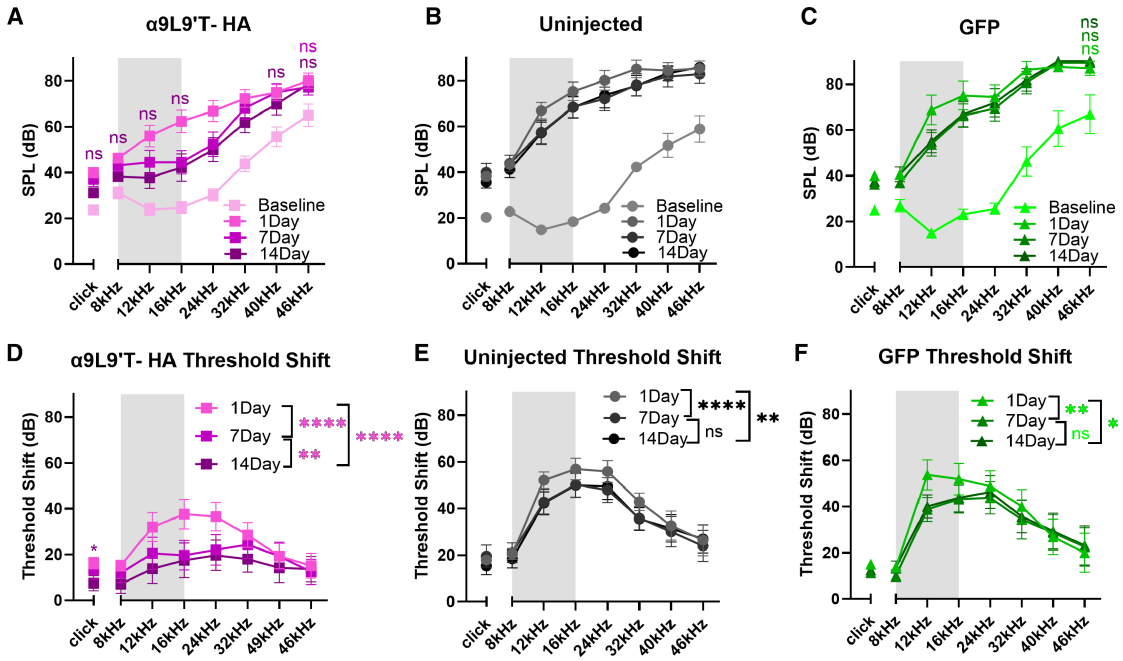

Figure 4. Threshold absolute values and shifts from baseline at 1, 7, and 14 days post exposure per group

Threshold (A–C) absolute values and (D–F) shifts from baseline. All animals were exposed to an octave-band (8–16 kHz) stimulus at 100 dB for 1 h, represented by the gray area on the frequency band. α9L9′T-HA injected group $N = 19$ (magenta), uninjected group $N = 14$ (black), GFP-injected group $N = 8$ (green). Different color intensities represent different time points, and same-color asterisks compare post-exposure time points to baseline of that group. Non-significant (ns) points are depicted as indicators of protection or recovery from acoustic damage. Values are mean ± SEM. (A–C) For clicks, Friedman's test with Dunn's multiple comparisons test; for pure tones, repeated measures two-way ANOVA with Dunnett's multiple comparisons test. (D–F) For clicks, Friedman's test with Dunn's multiple comparisons test; for pure tones, repeated-measures two-way ANOVA with Tukey's multiple comparisons test. *$p < 0.05$, **$p < 0.01$, ***$p < 0.001$, ****$p < 0.000$; ns, not significant.

DISCUSSION

Previous work has shown that heterozygous α9L9′T knockin mice have greatly enhanced efferent effects such as suppression of distortion product otoacoustic emissions and acoustic protection from noise exposure compared to wild type,[20,33] raising the possibility that the wild-type subunit can combine with the α9L9′T to form functional $(\alpha9)_2(\alpha10)_3$ nAChRs. On that basis, the present studies were undertaken to determine whether virally expressed nAChR subunits could insert significantly into wild-type synaptic complexes. Indeed such integrated expression did occur, as shown both by immunolabeling of an HA tag and by functional measures (slight baseline elevation and significant post-noise protection).

α9L9′T-HA was localized to the OHC postsynaptic membrane after AAV2.7m8 transduction with the transgene under a strong CAG promoter (Figure 1).[34,36] On the injected side (left), postsynaptic HA puncta in OHCs and cytoplasmic HA immunolabel of IHCs was greatest in apical segments and declined toward the base. This pattern would result if virus could only access hair cells in the organ of Corti via the scala tympani but not from the endolymph across the tight junctions of the reticular lamina. As shown by dye-tracking studies,[37] injection into the posterior semicircular canal spreads through perilymph to scala vestibuli and the cochlear helicotrema, entering the scala tympani at the cochlear apex. Only then can virus access the hair cell membrane via fluid exchange between the scala tympani and the organ of Corti. Thus, apical hair cells see the highest concentration of virus. Diffusional arguments also explain the opposite HA-expression gradient observed for IHCs in the contralateral cochlea. Here, viral crossover from the injected side to the contralateral cochlea occurs through the aqueduct that drains the perilymph into the subarachnoid space and inserts close to the base of the cochlea, especially in mouse pups that have a patent aqueduct at this age.[38–40] Thus, the basal contralateral cochlea sees the highest concentration of virus.[37]

We are not able to determine whether such low contralateral expression has any functional effect or, if it does, what its contribution is to ABR thresholds (only one HA-labeled contralateral OHC was found in two cochleas). Our ABR recordings were carried out with an open-field speaker, so it is probable that there is bilateral contribution to the ABR waveform. However, we only recorded (placed the recording electrode) from the left (injected) ear. We expect that wave 1 represents primarily the left cochlear nerve activity. Even if the contralateral ear was affected, that would not change the overall message of this study, i.e., that viral transduction of a gain-of-function nAChR prevents threshold changes after noise exposure.

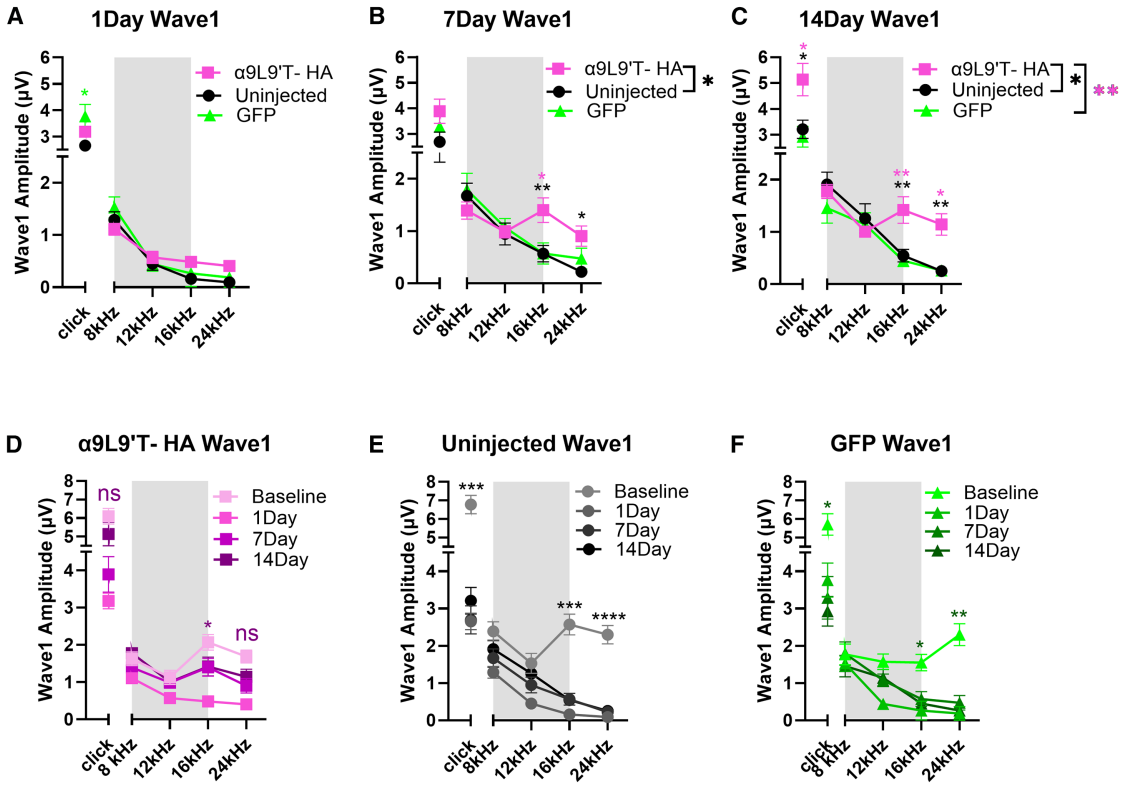

Figure 5. ABR wave-1 amplitude at 80 dB (μV) for clicks and pure tones

All animals were exposed to an octave-band (8–16 kHz) stimulus at 100 dB for 1 h, represented by the gray area. α9L9′T-HA injected group $N = 19$ (magenta), uninjected group $N = 14$ (black), GFP-injected group $N = 8$ (green). Values are mean ± SEM. (A–C) 1, 7, and 14 days post-exposure comparisons between groups. Black asterisks for uninjected vs. α9L9′T-HA, magenta asterisks for GFP vs. α9L9′T-HA, green asterisks for GFP vs. uninjected. For clicks, ordinary one-way ANOVA with Tukey's multiple comparisons test; for pure tones, two-way ANOVA with Tukey's multiple comparisons test. (D–F) Within-group comparisons. Different-color intensities represent different time points, and same-color asterisks compare post-exposure time points to baseline of that group. For clicks, repeated-measures one-way ANOVA with Dunnett's multiple comparisons test; for pure tones, repeated-measures two-way ANOVA with Dunnett's multiple comparisons test. Non-significant (ns) points are indicators of protection or recovery from acoustic damage. Multiplicity adjusted p values of 14-day vs. baseline comparisons for clicks, 16 Hz, and 24 kHz are plotted. *$p < 0.05$, **$p < 0.01$, ***$p < 0.001$, ****$p < 0.0001$; ns, not significant.

At 1, 7, and 14 days post exposure, both ABR absolute values and threshold shifts from baseline were significantly lower for the experimental α9L9′T-HA-injected mice vs. the control groups (Figure 3). The protective effect was greatest in the 12- to 32-kHz frequency range, where maximal damage occurs basal to the noise band used for acoustic trauma.[41–43] This corresponds to the middle cochlear turn, where efferent innervation density is greatest and α9L9′T-HA subunit expression is expected to have the greatest impact. With time after noise exposure, the α9L9′T-HA group showed accelerated recovery from day 1 to day 14 post exposure compared to control groups (Figures 3 and 4). This suggests that enhanced efferent feedback has the potential to prevent to some degree the progression from temporary threshold shift (TTS) to PTS. This is reminiscent of observations made in mouse lines where equivalent acoustic trauma produced only TTS in wild-type but PTS in α9 knockout mice.[20]

Click wave-1 amplitudes at 80 dB SPL in all groups declined 1 day after acoustic trauma, with minimal recovery thereafter for the control groups (Figure 5). At 14 days post trauma, the α9L9′T-HA group had prominent recovery of wave-1 amplitudes, reaching pre-trauma amplitude values, while the control groups remained reduced (∼50% of baseline values) (Figures 5 and 6). For a saturating (producing maximal activation of IHC afferents)[44,45] broadband (such as a click) acoustic stimulus, wave-1 amplitude at 80 dB SPL reflects the number of activatable type I cochlear afferents (viable IHC synapses and afferent neurons).[46–52] Presuming that a click at 80 dB is saturating, the improved recovery of wave-1 amplitude for the α9L9′T-HA group compared to controls shows that IHC to afferent transmission was preserved and protected from permanent damage. Pure-tone wave-1 amplitude at 80 dB data showed a similar pattern at 16–32 kHz, where the α9L9′T-HA group's amplitudes recovered over time, while the controls' amplitudes remained small.

To probe IHC function further, ribbon synapses were counted 15–17 days after acoustic trauma (Figure 7). However, no statistically significant differences in synapse number were found as a function

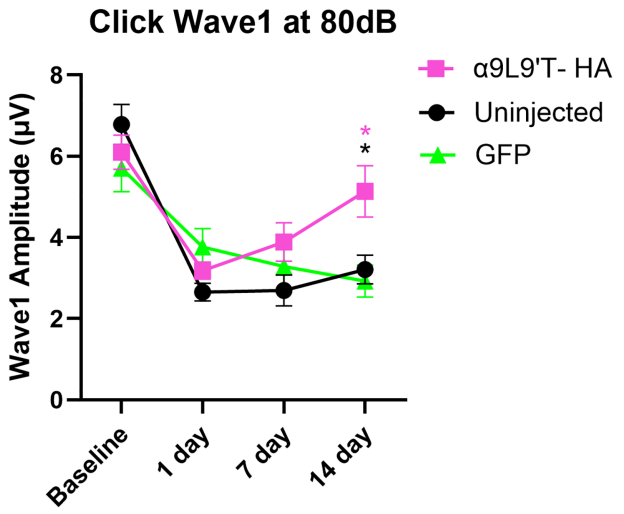

Figure 6. Click wave-1 amplitude at 80 dB recovery over time

Values are mean ± SEM. Repeated-measures two-way ANOVA with Tukey's multiple comparisons test showed that at 14 days, the α9L9′T-HA group was significantly larger than the controls (α9L9′T-HA vs. uninjected $p = 0.034$, α9L9′T-HA vs. GFP $p = 0.018$), showing progressive recovery, with no significant difference between pre-exposure and 14-day values ($p = 0.392$). α9L9′T-HA-injected group $N = 19$ (magenta), uninjected group $N = 14$ (black), GFP-injected group $N = 8$ (green). Black asterisks for uninjected vs. α9L9′T-HA, magenta asterisks for GFP vs. α9L9′T-HA. *$p < 0.05$, **$p < 0.01$, ***$p < 0.001$, ****$p < 0.0001$; ns, not significant.

of experimental group. This is perhaps not surprising, since synapse counts were quite variable. Although the absolute synapse numbers may not be significantly different, synaptic function and perhaps afferent fiber type distribution (high vs. low spontaneous rate) may be different among the groups post trauma. Noise-induced damage also targets other structures preceding IHC afferent synapses. For example, damage to stereocilia[53] could result in smaller voltage changes activating fewer voltage-gate calcium channels in IHCs. It will be of interest to explore post-trauma IHC synaptic function and stereocilia morphology in greater detail.

This work is motivated by the possibility of "efferent gene therapy" as a therapeutic strategy. Is this feasible? Gene therapy for inner ear disease has advanced significantly, largely to correct "deafness genes" that underlie inherited hearing loss. Notably, clinical trials for replacement or editing of mutant otoferlin (DFNB9) are under way in several countries.[54,55] Additional strategies to prevent or ameliorate ototoxic damage (such as from antibiotics or chemotherapeutics) seek small molecules to address mitochondrial function, generation of reactive oxygen species, or aspects of calcium excitotoxicity.[56] Prevention or reduction of noise-induced hearing loss, however, remains largely the domain of protective coverings or avoidance of acoustic trauma.[7] Small molecules such as positive allosteric modulators are being considered to increase hair cell nAChR gating, thereby enhancing acoustic protection.[57–59] Any future therapeutic must cross the blood/labyrinth barrier and avoid deleterious central nervous system side effects. This may be a smaller problem due to the unique pharmacology and restricted expression of α9α10 nAChRs, which have not been shown to function elsewhere in the nervous system.[60] However, a significant body of evidence has shown α9 expression in lymphocytes and has implicated their activity in inflammatory pain.[61–65]

α9L9′T intracochlear injections should eventually be assessed for systemic adverse events and effects on other sites apart from the OHCs, such as the aforementioned immune system and pain neural pathways. The therapeutic potential of the effects on pain modulation and the immune system are being studied.[63–65] An advantage of intracochlear gene therapy is local administration in a partially immune-privileged compartment such as the perilymphatic space. This means that smaller dosages are required to achieve therapeutic concentrations, where, even if the virus breaks the blood-labyrinth barrier, the risk of systematic interactions is diminished.[66] Further improvement will be possible using an OHC-specific promoter, such as for the gene *prestin*, that would greatly minimize transduction of other cell types and off-target effects. That being said, non-human primates that receive AAV intracochlear injections and were previously immunologically naive to the virus, as determined by undetectable anti-AAV antibody titers pre-injection, seroconvert after injection. Viral copies were also detected with droplet-digital PCR in cerebrospinal fluid, liver, and spleen, but without any laboratory or histological evidence of systemic toxicity.[67] With human gene therapy clinical trials under way, systemic adverse effects of AAV cochlear injections remain an open field of study.

Such concerns will be greater if regular dosing is required for protection from daily exposure to noise. This is clearly an issue for small-molecule therapies. However, it is not certain that repeated viral injections will be necessary. Animal and emerging human data show that expression can be maintained for more than 10 years.[68]

Thus, a local and targeted gene-therapy strategy does offer advantages. The drawbacks are that viral injection is time consuming, requires surgical expertise, and is intimidating compared to an oral or injectable medication. Nonetheless, the risk/benefit profile might be compared favorably to that for cochlear implants, where the surgical risks are higher but the benefit well established. Should efferent gene therapy be effective, the benefit for those at risk of early-onset presbycusis and unavoidable noise exposure may justify the additional challenges. A second potential application is for those suffering painful hyperacusis, or noxacusis. If, as proposed, type II cochlear afferents signal acoustic pain,[69–72] enhanced efferent inhibition of glutamate release from OHCs onto type II afferents may be particularly beneficial for this condition.

MATERIALS AND METHODS

Study design

The objectives of the study were to determine whether viral application would successfully transduce wild-type murine cochleas with the α9L9′T-HA subunit. This was confirmed by immunohistological

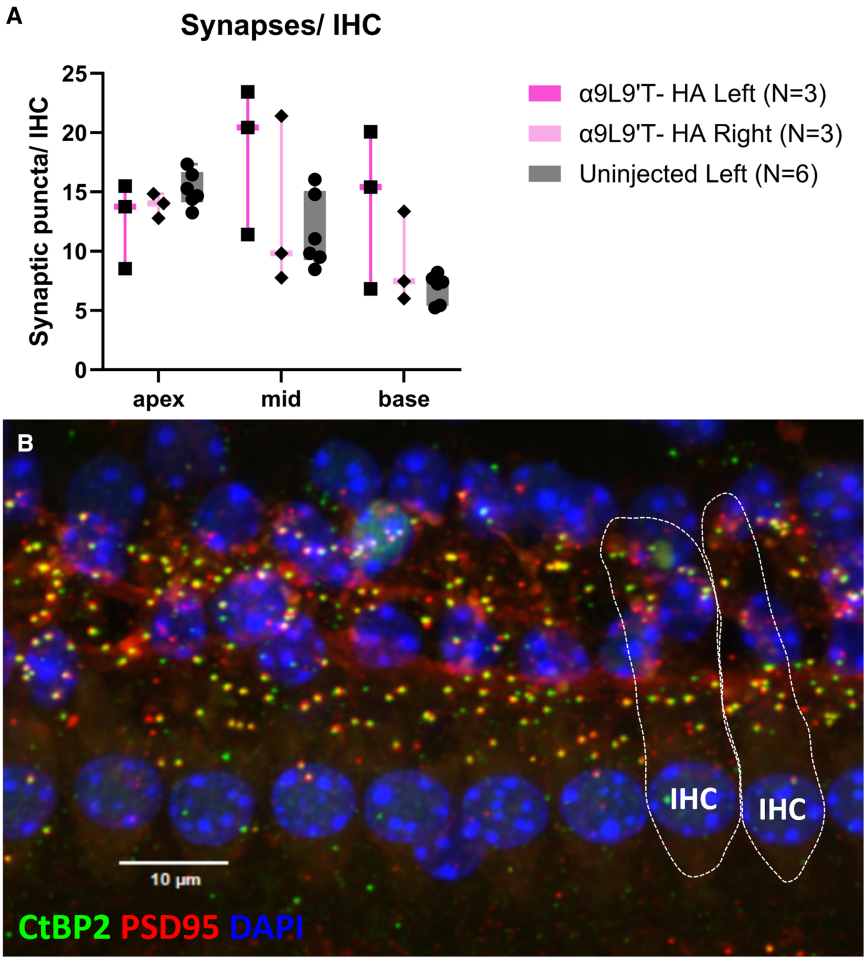

Figure 7. IHC afferent synapse counts

(A) Synapses/IHCs for the apical, middle, and basal area of the left α9L9′T-HA-injected cochleas, the right uninjected α9L9′T-HA side, and the left cochleas of the uninjected group. Confocal images of every cochlear region, with 15–30 IHCs per image, were acquired. Co-localized immunolabeled CtBP2/PSD95 puncta were counted and divided by the number of IHC nuclei stained with DAPI. Mean ± maximum, minimum, and individual values. Two-way ANOVA showed no difference between groups in all cochlear regions. (B) Representative maximum-intensity projection image of co-localized CtBP2 (green)/PSD95 (red) synaptic puncta from the left middle turn of an α9L9′T-HA-injected 7-week-old male C57Bl/J6 mouse. IHC nuclei are stained blue with DAPI, and cell margins are outlined with white dashed lines.

labeling of the HA tag on the postsynaptic OHC membrane juxtaposed to presynaptic efferent terminals labeled for SV2 (Figure 1). The functional implications of the gene therapy were studied by performing hearing assessment with ABR recordings. At baseline, the α9L9′T-HA subunit minimally affected auditory function (Figure 2). The primary goal was to study how the expression of the α9L9′T-HA subunit would affect the ABR response after traumatic exposure, compared to controls (Figures 3, 4, 5, and 6). Finally, IHC afferent synapses were labeled with immunofluorescent antibodies and counted to determine whether the observed findings would correlate with IHC afferent synapse counts at 14 days post exposure (Figure 7).

Wild-type C57Bl/J6 male and female mouse pups received left posterior semicircular canal injections at postnatal days 1–5 (P1–P5) with either AAV2.7m8-CAG-α9L9′T-HA or AAV2.7m8-CAG-eGFP virus. Uninjected littermates served as controls. The GFP-injected mice served as surgical and viral controls. At 5 weeks of age all mice were exposed to an octave-band signal (8–16 kHz) at 100 dB SPL for 1 h. Baseline ABRs were recorded 1–3 days prior to noise exposure and 1, 7, and 14 days post noise exposure. At 7 weeks of age, all mice were sacrificed and their cochleas fixed for immunohistological analysis.

This was a randomized experimental study. Treatment included posterior semicircular canal viral injection with AAV2.7m8-α9L9′T-HA. Mice were purpose bred for this study, and breeding was carried out independently. Mouse pups were assigned to an experimental group randomly and independently of any particular factor. Forty-one mice in total, 20 females and 21 males, were used. The α9L9′T-HA group included 19 mice (10 female and 9 male), the uninjected group included 14 mice (6 female and 8 male), and the GFP group included 8 mice (4 female and 4 male).

Sample size was determined based on previous experience and validated by the following equation:[73]

$$E = \text{Total number of animals minus the total number of groups} = 41 - 3 = 38.$$

Using the resource equation, there are 41 animals comprising three groups and E = 38, almost twice the recommended 20.

The experiments are reported according to ARRIVE guidelines.

α9L9′T-HA AAV2.7m8

Mouse α9L9′T-HA cDNA[35] was incorporated into a plasmid (Genewiz, South Plainfield, NJ) and submitted to the Penn Vector Core (Gene Therapy Program, University of Pennsylvania School of Medicine) for incorporation into AAV2.7m8[74] obtained from Addgene, University of California, Berkeley, MTA no. 486064. α9L9′T is the targeted mutation designated as Chrna9^{tm1Elgo} in MGI. The resulting

viral vector (AAV2.7m8.CAG.mChrnα9L9′THA.bGH) was provided for use at 1.73×10^{13} GC/mL. This was subdivided into 100-μL aliquots and stored at −80°C. Once thawed for use, each aliquot was stored at 4°C (not refrozen) until exhausted. AAV2.7m8-CAG-eGFP (9.75×10^{12} GC/mL), was donated by Wade Chien and constructed similarly: the CAG promoter derived from the InvivoGen pDRIVE CAG plasmid (InvivoGen, San Diego, CA), the cDNA encoding eGFP protein, and the bovine growth hormone polyadenylation signal.[31,34]

Mice

Care and housing of animals was in accordance with institutional guidelines as specified in Johns Hopkins Institutional Animal Care and Use Committee (IACUC) protocol MO23M04. C57Bl/J6 wild-type mice were used for this study. The breeders were purchased from The Jackson Laboratory and maintained in the Johns Hopkins University School of Medicine Research Animal Resource facility. Mice were placed on a 12:12-h light/dark cycle and housed in cages with water and autoclaved feed in a low-noise satellite facility without automated racks. All experiments were carried out under protocols approved by the IACUC protocol #MO23M04.

Animal surgery

Hypothermia was used to induce and maintain anesthesia. The posterior semicircular canal was exposed through a postauricular incision and tissue dissection. Only the left ear of each animal was injected. A nanoliter microinjection system (Nanoject III, Model #3-000-207, Drummond Scientific, Broomall, PA) was used. 400–1,100 nL of viral solution mixed with Fast Green dye (4:1) were injected into the left posterior semicircular canal using a glass micropipette (3.5 inches [90 mm], Drummond Scientific, #3-000-203-G/X) pulled to produce a tip opening of ∼20 μm. Viral load concentration injected was 1.38×10^{13} GC/mL (1.73×10^{13} GC/mL original concentration diluted by the dye). Therefore, for the range of volumes injected, this corresponds to a $5.54–15.22 \times 10^{9}$ GC range of viral copies.[34,75] The pipette was backfilled with mineral oil and the injection solution loaded into it prior to the surgery. The solution was injected in bouts of 100 nL at a rate of 50 nL/s. Once the injection was concluded, the pipette was removed and the tissue and skin were sutured back together. The pups were put on a heating pad for recovery. The wound site was disinfected with betadine and 70% ethanol, and the entire procedure was carried out under sterile conditions.

Auditory brainstem response

ABR measurements were conducted in a soundproofed booth (Industrial Acoustics Company, Bronx, NY; $59 \times 74 \times 60$ cm^3) lined with acoustic foam (Pinta Acoustic, Minneapolis, MN). Animals were anesthetized with intraperitoneal ketamine (100 mg/kg) and xylazine (20 mg/kg), and their eyes were swabbed with petrolatum-based ophthalmic ointment to prevent corneal ulcers. During the test they were placed on an infrared heating pad (Kent Scientific, Physio Suite, Modular System) to maintain a core temperature of 37°C. Subdermal needle electrodes (Disposable Horizon, 13-mm needle, Rochester Med, Coral Springs, FL) were placed on the left mastoid (active), vertex (reference), and hindlimb (ground) in a standard ABR recording arrangement. ABR signals were acquired with a Medusa4Z preamplifier (12 kHz sampling rate) and filtered from 300 to 3,000 Hz with an additional band-reject filter at 60 Hz. Clicks or pure-tone stimuli (512 repetitions, 10–90 dB in 10-dB steps, 21 stimuli/s) were used to generate averaged ABR waveforms. The duration of the tonal stimulus was 5 ms, with a 0.5-ms rise and fall time. Stimuli were created in SigGen software (Tucker-Davis Technologies [TDT], Alachua, FL) and generated by an RZ6 multi-I/O processor (TDT). Stimuli were played from a free field speaker (MF1, TDT) located 10 cm from the animal's left pinna at 0° azimuth. Stimuli were calibrated with a 0.25-inch (6.35 mm) free-field microphone (PCB Piezotronics, Depew, NY, model 378C01) placed at the location of the animal's pinna.

ABR traces were analyzed by two researchers independently, one of whom was completely blinded to the experimental conditions of the subjects. Inter-rater correspondence was >98%. ABR threshold was defined as the average between the lowest sound level to evoke a response and the first level with no response (any wave). Peak-to-trough wave-1 amplitudes were derived manually.

Acoustic exposure protocol

Awake, unrestrained mice were exposed to a 100-dB SPL octave-band (8–16 kHz) noise for 1 h. Mice were put into a custom-built soundproof chamber ($53.5 \times 54.5 \times 57$ cm) lined with 4-cm-thick Sonex sound attenuating foam (Illbruck) within individual wire cells ($10.5\text{cm} \times 5\text{ cm} \times 5$ cm), where they moved freely. A Fostex dome tweeter speaker (FT28D), mounted atop a chicken-wire bridge (0.5×0.5-inch [12.7×12.7 mm] squares) was suspended over the center of the mouse cage in the booth. The Fostex speaker was wired to an amplifier (Crown D-75A), which was hooked up to a Dell Optiplex computer (Model 580). The sound file was 5 min in duration and was presented on a continuous loop for the duration of the noise exposure (1 h). Calibrations were conducted using a Larson Davis sound-level meter (System 824) to ensure the noise was 100 dB (*Z*-weighted scale) in all four corners and in the center of the cage. Calibrations took place before every noise exposure.

Immunohistochemistry and quantification

After the 14-day ABRs concluded, mice were euthanized with isofluorane overdose followed by decapitation and both cochleas fixed in 4% paraformaldehyde for 30 min at room temperature. The cochleas were decalcified in 250 mM EDTA for 2–3 days at room temperature following dissection, then underwent blocking for immunohistology. Primary antibodies used are Cell Signaling Technology HA-Tag (C29F4) Rabbit mAb #3724 (1:100), DSHB Mouse IgG1 anti-SV2 (1:1,000), Biolegend Purified Mouse IgG2α,κ anti-PSD95 #810401 (Previously Covance catalog #MMS-5182) (1:200), and BD Transduction Laboratories # 612044 Clone 16 Purified Mouse IgG1 anti-CtBP2 (1:200). Secondary Alexa Fluor-conjugated antibodies from Invitrogen (1:1,000) were used with DAPI (1:2,000) to label the nuclei. Whole-mount cochlear segments were mounted with ProLong Gold antifade reagent (catalog #P36930, Thermo Fisher Scientific). Images

were acquired on an inverted Nikon A1 confocal microscope using 40× NA 1.3 and 63× NA 1.4 oil-immersion objectives. ImageJ/Fiji (RRID: SCR_002285) was used for image analysis and counts. Synaptic puncta were manually counted by one observer on the z stack of the whole mount. For IHC afferent synapse counts, only the juxtaposed green and red CtBP2/PSD-95 puncta were included.

Statistical analysis

Mean ± SEM are plotted. Data were analyzed with GraphPad Prism 10.2.3. Statistical analyses included the following. For clicks: if normality present, ordinary one-way ANOVA with Tukey's multiple comparisons test or repeated-measures one-way ANOVA with Dunnett's multiple comparisons test; if non-normal data, Kruskal-Wallis test or Friedman's test (if repeated measures) with Dunn's multiple comparisons. For pure tones, we used two-way ANOVA with multiplicity adjusted p values after Tukey's multiple comparisons test or repeated-measures two-way ANOVA with multiplicity adjusted p values after either Dunnett's or Tukey's tests. Two-way ANOVA was used for IHC synapse counts. Differences were considered statistically significant if $p < 0.05$.

DATA AND CODE AVAILABILITY

All data, including statistical validation, are included in the paper. Research materials are available via a Materials Transfer Agreement issued by the Johns Hopkins Office of Tech Transfer.

ACKNOWLEDGMENTS

We thank F. Chakir for outstanding technical support and Drs. H. Hiel and A. Lauer for guidance on histology and ABRs, respectively. We thank Dr W. Chien for continued generosity with the GFP virus. Support was provided by R01 DC001508 and R01 DC016559 from the National Institute on Deafness and Other Communication Disorders, NIH, by the David M. Rubenstein Professorship and Fund for Hearing Research at Johns Hopkins University School of Medicine, and by an Emerging Research grant from the Hearing Health Foundation to M.W.

AUTHOR CONTRIBUTIONS

Data collection was performed by E.S., analysis by E.S., P.A.F., and M.W., project direction by E.S., P.A.F., and M.W., funding acquisition by P.A.F. and M.W., writing of the original draft by E.S., and revisions and editing by E.S., P.A.F., and M.B.W.

DECLARATION OF INTERESTS

US and International Patent Application US2023/033849, filed 9/27/2023, "Cholinergic Gene Therapy to Preserve Hearing" (P.A.F.).

REFERENCES

1. Chadha, S., Kamenov, K., and Cieza, A. (2021). The world report on hearing, 2021. Bull. World Health Organ. *99*. 242–242A.
2. GBD 2019 Hearing Loss Collaborators (2021). Hearing loss prevalence and years lived with disability, 1990–2019: findings from the Global Burden of Disease Study 2019. Lancet (London, England) *397*, 996–1009.
3. McDaid, D., Park, A.-L., and Chadha, S. (2021). Estimating the global costs of hearing loss. Int. J. Audiol. *60*, 162–170.
4. Orji, A., Kamenov, K., Dirac, M., Davis, A., Chadha, S., and Vos, T. (2020). Global and regional needs, unmet needs and access to hearing aids. Int. J. Audiol. *59*, 166–172.
5. Scholes, S., Biddulph, J., Davis, A., and Mindell, J.S. (2018). Socioeconomic differences in hearing among middle-aged and older adults: cross-sectional analyses using the Health Survey for England. BMJ Open *8*, e019615.
6. Basner, M., Babisch, W., Davis, A., Brink, M., Clark, C., Janssen, S., and Stansfeld, S. (2014). Auditory and non-auditory effects of noise on health. Lancet *383*, 1325–1332.
7. Natarajan, N., Batts, S., and Stankovic, K.M. (2023). Noise-Induced Hearing Loss. J. Clin. Med. *12*, 2347.
8. Carroll, Y.I., Eichwald, J., Scinicariello, F., Hoffman, H.J., Deitchman, S., Radke, M. S., Themann, C.L., and Breysse, P. (2017). Vital Signs: Noise-Induced Hearing Loss Among Adults — United States 2011–2012. MMWR Morb. Mortal. Wkly. Rep. *66*, 139–144.
9. Hammer, M.S., Swinburn, T.K., and Neitzel, R.L. (2014). Environmental noise pollution in the United States: developing an effective public health response. Environ. Health Perspect. *122*, 115–119.
10. Fuchs, P.A., and Lauer, A.M. (2019). Efferent Inhibition of the Cochlea. Cold Spring Harb. Perspect. Med. *9*, a033530.
11. Warr, W.B., and Guinan, J.J., Jr. (1979). Efferent innervation of the organ of corti: two separate systems. Brain Res. *173*, 152–155.
12. Roux, I., Wersinger, E., McIntosh, J.M., Fuchs, P.A., and Glowatzki, E. (2011). Onset of Cholinergic Efferent Synaptic Function in Sensory Hair Cells of the Rat Cochlea. J. Neurosci. *31*, 15092–15101.
13. Vattino, L.G., Wedemeyer, C., Elgoyhen, A.B., and Katz, E. (2020). Functional Postnatal Maturation of the Medial Olivocochlear Efferent–Outer Hair Cell Synapse. J. Neurosci. *40*, 4842–4857.
14. Johnson, S.L., Wedemeyer, C., Vetter, D.E., Adachi, R., Holley, M.C., Elgoyhen, A.B., and Marcotti, W. (2013). Cholinergic efferent synaptic transmission regulates the maturation of auditory hair cell ribbon synapses. Open Biol. *3*, 130163.
15. Sato, M., Henson, M.M., and Smith, D.W. (1997). Synaptic specializations associated with the outer hair cells of the Japanese macaque. Hear. Res. *108*, 46–54.
16. Smith, C.A., and Sjostrand, F.S. (1961). Structure of the nerve endings on the external hair cells of the guinea pig cochlea as studied by serial sections. J. Ultrastruct. Res. *5*, 523–556.
17. Fuchs, P.A., Lehar, M., and Hiel, H. (2014). Ultrastructure of Cisternal Synapses on Outer Hair Cells of the Mouse Cochlea. J. Comp. Neurol. *522*, 717–729.
18. Wersinger, E., McLean, W.J., Fuchs, P.A., and Pyott, S.J. (2010). BK Channels Mediate Cholinergic Inhibition of High Frequency Cochlear Hair Cells. PLoS One *5*, e13836.
19. Elgoyhen, A.B., and Katz, E. (2012). The efferent medial olivocochlear-hair cell synapse. J. Physiol. Paris *106*, 47–56.
20. Boero, L.E., Castagna, V.C., Di Guilmi, M.N., Goutman, J.D., Elgoyhen, A.B., and Gómez-Casati, M.E. (2018). Enhancement of the Medial Olivocochlear System Prevents Hidden Hearing Loss. J. Neurosci. *38*, 7440–7451.
21. Chumak, T., Bohuslavova, R., Macova, I., Dodd, N., Buckiova, D., Fritzsch, B., Syka, J., Pavlinkova, G., Chumak, T., Bohuslavova, R., et al. (2016). Deterioration of the Medial Olivocochlear Efferent System Accelerates Age-Related Hearing Loss in Pax2-Isl1 Transgenic Mice. Mol. Neurobiol. *53*, 2368–2383.
22. Galambos, R. (1956). Suppression of auditory nerve activity by stimulation of efferent fibers to cochlea. J. Neurophysiol. *19*, 424–437.
23. Kujawa, S.G., and Liberman, M.C. (1997). Conditioning-Related Protection From Acoustic Injury: Effects of Chronic Deefferentation and Sham Surgery. J. Neurophysiol. *78*, 3095–3106.
24. Liberman, M.C. (1991). The olivocochlear efferent bundle and susceptibility of the inner ear to acoustic injury. J. Neurophysiol. *65*, 123–132.
25. Liberman, M.C., Liberman, L.D., and Maison, S.F. (2014). Efferent Feedback Slows Cochlear Aging. J. Neurosci. *34*, 4599–4607.
26. Maison, S.F., and Liberman, M.C. (2000). Predicting Vulnerability to Acoustic Injury with a Noninvasive Assay of Olivocochlear Reflex Strength. J. Neurosci. *20*, 4701–4707.
27. Maison, S.F., Luebke, A.E., Liberman, M.C., and Zuo, J. (2002). Efferent Protection from Acoustic Injury Is Mediated via α9 Nicotinic Acetylcholine Receptors on Outer Hair Cells. J. Neurosci. *22*, 10838–10846.

28. Maison, S.F., Usubuchi, H., and Liberman, M.C. (2013). Efferent Feedback Minimizes Cochlear Neuropathy from Moderate Noise Exposure. J. Neurosci. *33*, 5542–5552.
29. Reiter, E.R., and Liberman, M.C. (1995). Efferent-mediated protection from acoustic overexposure: relation to slow effects of olivocochlear stimulation. J. Neurophysiol. *73*, 506–514.
30. Wiederhold, M.L., and Kiang, N.Y. (1970). Effects of Electric Stimulation of the Crossed Olivocochlear Bundle on Single Auditory-Nerve Fibers in the Cat. J. Acoust. Soc. Am. *48*, 950–965.
31. Zhang, Y., Hiel, H., Vincent, P.F.Y., Wood, M.B., Elgoyhen, A.B., Chien, W., Lauer, A., and Fuchs, P.A. (2023). Engineering olivocochlear inhibition to reduce acoustic trauma. Mol. Ther. Methods Clin. Dev. *29*, 17–31.
32. Plazas, P.V., De Rosa, M.J., Gomez-Casati, M.E., Verbitsky, M., Weisstaub, N., Katz, E., Bouzat, C., and Elgoyhen, A.B. (2005). Key roles of hydrophobic rings of TM2 in gating of the alpha9alpha10 nicotinic cholinergic receptor. Br. J. Pharmacol. *145*, 963–974.
33. Taranda, J., Maison, S.F., Ballestero, J.A., Katz, E., Savino, J., Vetter, D.E., Boulter, J., Liberman, M.C., Fuchs, P.A., and Elgoyhen, A.B. (2009). A point mutation in the hair cell nicotinic cholinergic receptor prolongs cochlear inhibition and enhances noise protection. PLoS Biol. *7*, e18.
34. Isgrig, K., McDougald, D.S., Zhu, J., Wang, H.J., Bennett, J., and Chien, W.W. (2019). AAV2.7m8 is a powerful viral vector for inner ear gene therapy. Nat. Commun. *10*, 427.
35. Vyas, P., Wood, M.B., Zhang, Y., Goldring, A.C., Chakir, F.Z., Fuchs, P.A., and Hiel, H. (2020). Characterization of HA-tagged α9 and α10 nAChRs in the mouse cochlea. Sci. Rep. *10*, 21814.
36. Zhu, J., Choi, J.W., Ishibashi, Y., Isgrig, K., Grati, M., Bennett, J., and Chien, W. (2021). Refining surgical techniques for efficient posterior semicircular canal gene delivery in the adult mammalian inner ear with minimal hearing loss. Sci. Rep. *11*, 18856.
37. Talaei, S., Schnee, M.E., Aaron, K.A., and Ricci, A.J. (2019). Dye Tracking Following Posterior Semicircular Canal or Round Window Membrane Injections Suggests a Role for the Cochlea Aqueduct in Modulating Distribution. Front. Cell. Neurosci. *13*, 471.
38. Stöver, T., Yagi, M., and Raphael, Y. (2000). Transduction of the contralateral ear after adenovirus-mediated cochlear gene transfer. Gene Ther. *7*, 377–383.
39. Plontke, S.K., and Salt, A.N. (2018). Local drug delivery to the inner ear: Principles, practice, and future challenges. Hear. Res. *368*, 1–2.
40. Salt, A.N., and Hirose, K. (2018). Communication pathways to and from the inner ear and their contributions to drug delivery. Hear. Res. *362*, 25–37.
41. Hesse, L.L., Bakay, W., Ong, H.-C., Anderson, L., Ashmore, J., McAlpine, D., Linden, J., and Schaette, R. (2016). Non-Monotonic Relation Between Noise Exposure Severity and Neuronal Hyperactivity in the Auditory Midbrain. Front. Neurol. *7*, 133.
42. Gittleman, S.N., Prell, C.G.L., and Hammill, T.L. (2019). Octave band noise exposure: Laboratory models and otoprotection efforts. J. Acoust. Soc. Am. *146*, 3800.
43. Kujawa, S.G., and Liberman, M.C. (2015). Synaptopathy in the noise-exposed and aging cochlea: primary neural degeneration in acquired sensorineural hearing loss. Hear. Res. *330*, 191–199.
44. Chatterjee, M., and Zwislocki, J.J. (1998). Cochlear mechanisms of frequency and intensity coding. II. Dynamic range and the code for loudness. Hear. Res. *124*, 170–181.
45. Dallos, P. (1985). Response characteristics of mammalian cochlear hair cells. J. Neurosci. *5*, 1591–1608.
46. Cheatham, M.A., Huynh, K.H., Gao, J., Zuo, J., and Dallos, P. (2004). Cochlear function in Prestin knockout mice. J. Physiol. *560*, 821–830.
47. Fernandez, K.A., Guo, D., Micucci, S., Gruttola, V.D., Liberman, M.C., and Kujawa, S.G. (2020). Noise-induced Cochlear Synaptopathy with and Without Sensory Cell Loss. Neuroscience *427*, 43–57.
48. Kujawa, S.G., and Liberman, M.C. (2009). Adding Insult to Injury: Cochlear Nerve Degeneration after "Temporary" Noise-Induced Hearing Loss. J. Neurosci. *29*, 14077–14085.
49. Hickox, A.E., Larsen, E., Heinz, M.G., Shinobu, L., and Whitton, J.P. (2017). Translational issues in cochlear synaptopathy. Hear. Res. *349*, 164–171.
50. Lin, H.W., Furman, A.C., Kujawa, S.G., and Liberman, M.C. (2011). Primary neural degeneration in the Guinea pig cochlea after reversible noise-induced threshold shift. J. Assoc. Res. Otolaryngol. *12*, 605–616.
51. Negandhi, J., Harrison, A.L., Allemang, C., and Harrison, R.V. (2014). Time course of cochlear injury discharge (excitotoxicity) determined by ABR monitoring of contralateral cochlear events. Hear. Res. *315*, 34–39.
52. Hu, N., Rutherford, M.A., and Green, S.H. (2020). Protection of cochlear synapses from noise-induced excitotoxic trauma by blockade of Ca(2+)-permeable AMPA receptors. Proc. Natl. Acad. Sci. USA *117*, 3828–3838.
53. Wagner, E.L., and Shin, J.-B. (2019). Mechanisms of hair cell damage and repair. Trends Neurosci. *42*, 414–424.
54. Lv, J., Wang, H., Cheng, X., Chen, Y., Wang, D., Zhang, L., Cao, Q., Tang, H., Hu, S., Gao, K., et al. (2024). AAV1-hOTOF gene therapy for autosomal recessive deafness 9: a single-arm trial. Lancet *403*, 2317–2325.
55. Qi, J., Tan, F., Zhang, L., Lu, L., Zhang, S., Zhai, Y., Lu, Y., Qian, X., Dong, W., Zhou, Y., et al. (2024). AAV-Mediated Gene Therapy Restores Hearing in Patients with DFNB9 Deafness. Adv. Sci. *11*, e2306788.
56. Wu, P., Barros-Becker, F., Ogelman, R., Camci, E.D., Linbo, T.H., Simon, J.A., Rubel, E.W., and Raible, D.W. (2024). Multiple mechanisms of aminoglycoside ototoxicity are distinguished by subcellular localization of action. Front. Neurol. *15*, 1480435.
57. Elgoyhen, A.B. (2022). The α9α10 nicotinic acetylcholine receptor: a compelling drug target for hearing loss? Expert Opin. Ther. Targets *26*, 291–302.
58. Wang, J., and Lindstrom, J. (2018). Orthosteric and allosteric potentiation of heteromeric neuronal nicotinic acetylcholine receptors. Br. J. Pharmacol. *175*, 1805–1821.
59. Gu, S., Knowland, D., Matta, J.A., O'Carroll, M.L., Davini, W.B., Dhara, M., Kweon, H.-J., and Bredt, D.S. (2020). Hair cell α9α10 nicotinic acetylcholine receptor functional expression regulated by ligand binding and deafness gene products. Proc. Natl. Acad. Sci. USA *117*, 24534–24544.
60. Morley, B.J., Whiteaker, P., and Elgoyhen, A.B. (2018). Commentary: Nicotinic Acetylcholine Receptor α9 and α10 Subunits Are Expressed in the Brain of Mice. Front. Cell. Neurosci. *12*, 104.
61. Christensen, S.B., Hone, A.J., Roux, I., Kniazeff, J., Pin, J.-P., Upert, G., Servent, D., Glowatzki, E., and McIntosh, J.M. (2017). RgIA4 Potently Blocks Mouse α9α10 nAChRs and Provides Long Lasting Protection against Oxaliplatin-Induced Cold Allodynia. Front. Cell. Neurosci. *11*, 219.
62. Hone, A.J., and McIntosh, J.M. (2018). Nicotinic Acetylcholine Receptors in Neuropathic and Inflammatory Pain. FEBS Lett. *592*, 1045–1062.
63. Hone, A.J., Servent, D., and McIntosh, J.M. (2018). α9-containing nicotinic acetylcholine receptors and the modulation of pain. Br. J. Pharmacol. *175*, 1915–1927.
64. Shelukhina, I., Siniavin, A., Kasheverov, I., Ojomoko, L., Tsetlin, V., and Utkin, Y. (2023). α7- and α9-Containing Nicotinic Acetylcholine Receptors in the Functioning of Immune System and in Pain. Int. J. Mol. Sci. *24*, 6524.
65. McIntosh, J.M., Absalom, N., Chebib, M., Elgoyhen, A.B., and Vincler, M. (2009). Alpha9 nicotinic acetylcholine receptors and the treatment of pain. Biochem. Pharmacol. *78*, 693–702.
66. Landegger, L.D., Reisinger, E., Lallemend, F., Hage, S.R., Grimm, D., and Cederroth, C.R. (2024). The rise of cochlear gene therapy. Mol. Ther. https://doi.org/10.1016/j.ymthe.2024.11.012.
67. Andres-Mateos, E., Landegger, L.D., Unzu, C., Phillips, J., Lin, B.M., Dewyer, N.A., Sanmiguel, J., Nicolaou, F., Valero, M.D., Bourdeu, K.I., et al. (2022). Choice of vector and surgical approach enables efficient cochlear gene transfer in nonhuman primate. Nat. Commun. *13*, 1359.
68. Muhuri, M., Levy, D.I., Schulz, M., McCarty, D., and Gao, G. (2022). Durability of transgene expression after rAAV gene therapy. Mol. Ther. *30*, 1364–1380.
69. Nowak, N., Wood, M.B., Glowatzki, E., and Fuchs, P.A. (2021). Prior Acoustic Trauma Alters Type II Afferent Activity in the Mouse Cochlea. eNeuro *8*. ENEURO.0383-21.2021.

70. Wood, M.B., Nowak, N., and Fuchs, P.A. (2024). Frontiers | Damage-evoked signals in cochlear neurons and supporting cells. Front. Neurol. *15*, 1361747.

71. Liu, C., Glowatzki, E., and Fuchs, P.A. (2015). Unmyelinated type II afferent neurons report cochlear damage. Proc. Natl. Acad. Sci. USA *112*, 14723–14727.

72. Weisz, C.J.C., Williams, S.-P.G., Eckard, C.S., Divito, C.B., Ferreira, D.W., Fantetti, K.N., Dettwyler, S.A., Cai, H.-M., Rubio, M.E., Kandler, K., and Seal, R.P. (2021). Outer Hair Cell Glutamate Signaling through Type II Spiral Ganglion Afferents Activates Neurons in the Cochlear Nucleus in Response to Nondamaging Sounds. J. Neurosci. *41*, 2930–2943.

73. Charan, J., and Kantharia, N.D. (2013). How to calculate sample size in animal studies? J. Pharmacol. Pharmacother. *4*, 303–306.

74. Dalkara, D., Byrne, L.C., Klimczak, R.R., Visel, M., Yin, L., Merigan, W.H., Flannery, J.G., and Schaffer, D.V. (2013). In Vivo–Directed Evolution of a New Adeno-Associated Virus for Therapeutic Outer Retinal Gene Delivery from the Vitreous. Sci. Transl. Med. *5*, 189ra76.

75. Tao, Y., Huang, M., Shu, Y., Ruprecht, A., Wang, H., Tang, Y., Vandenberghe, L.H., Wang, Q., Gao, G., Kong, W.J., and Chen, Z.Y. (2018). Delivery of Adeno-Associated Virus Vectors in Adult Mammalian Inner-Ear Cell Subtypes Without Auditory Dysfunction. Hum. Gene Ther. *29*, 492–506.